Three-dimensional pore characterization of poly(lactic)acid/bamboo biodegradable panels

Dang Mao Nguyen, Thi My Hanh Diep, Yuri Ferreira da Silva, Thi Nhung Vu, Dongquy Hoang, Chi Nhan Ha Thuc, Quoc Bao Bui, Patrick Perré

Three-dimensional pore characterization of poly(lactic)acid/bamboo biodegradable panels

Dang Mao Nguyen[1], Thi My Hanh Diep[2,3], Yuri Ferreira da Silva[4,5], Thi Nhung Vu[3,6], DongQuy Hoang[3,6], Chi Nhan Ha Thuc[3,6], Quoc Bao Bui[7*], Patrick Perré[5]

[1]Laboratoire Innovation Matériau Bois Habitat Apprentissage (LIMBHA), Ecole Supérieure du Bois, 7 Rue Christian Pauc, 44306 Nantes, France

[2]Center Research for Natural Resources Conservation, University of Science, Ho Chi Minh City, Vietnam

[3]Vietnam National University, Ho Chi Minh City 700000, Vietnam

[4]Laboratory of Surfaces Engineering, Department of Metallurgical and Materials Engineering, COPPE, Federal University of Rio de Janeiro, P.O. Box: 68505, 21945-970, Rio de Janeiro, RJ, Brazil

[5]Université Paris-Saclay, CentraleSupélec, Laboratoire de Génie des Procédés et Matériaux, SFR Condorcet FR CNRS 3417, Centre Européen de Biotechnologie et de Bioéconomie (CEBB), 3 rue des Rouges Terres 51110 Pomacle, France

[6]Faculty of Materials Science and Technology, University of Science, Ho Chi Minh City 700000, Vietnam

[7]Sustainable Developments in Civil Engineering Research Group, Faculty of Civil Engineering, Ton Duc Thang University, Ho Chi Minh City, Vietnam

*Correspondance : buiquocbao@tdtu.edu.vn (Q-B Bui)

Abstract

In the context of novel environmental and energy regulations in construction (RE2020), biocomposites derived from bamboo fibers, bamboo powders, and biodegradable poly(lactic)acid polymer, all of which are renewable resources, have been investigated to meet the criteria of the novel regulations. In this work, the biocomposites were manufactured by twin-screw internal mixing at 170°C for 5 minutes with a rotation speed of 60 rpm. The composites sheets were then shaped on a hydraulic press at 185°C. Pore characterization including pore volume fraction, 3D-pore structure and morphology, and pore distribution of these materials were investigated using X-ray tomography combined with image processing (Avizo). The results show that when the bamboo fibers content is increased, an augmentation in the pore volume fraction and the number of large-volume pores could be observed. In turn, the bamboo powder-containing sheet had a significant increase in pore volume fraction, while a higher quantity of smaller pores, with uniform size, could be observed. The water absorption capacity of these composite increases with the increase of the amount of pore distribution, pore connection, and pore volume fraction. In addition, the orientation of the fibers in 3D observation, flexural mechanical properties, and thermal stability of the biocomposites are also reported in this study.

Keywords: biocomposites; 3D pore properties; X-ray tomography; bamboo fibers/powders; image processing.

1. Introduction

Buildings are responsible for about 36% of global energy consumption and generate about 40-50% of global greenhouse gas emissions during construction [1, 2]. In this

context, a succession of thermal regulations (RT2000, RT2005, RT2012) has been introduced with increasing thermal objectives to reduce the energy consumption of buildings and promote green construction. Similarly, important evolution, the last norm, the RE2020 regulation, introduced the concept of eco-design, by introducing new environmental standards for future construction to reduce the global emissions of the building sector. Europe is no exception, with carbon neutrality targeted by it in 2050. Moreover, France takes part in the Energy Transition for Green Growth law, therefore requiring major changes within the sector. The environmental regulations for the new construction of buildings in France (RE2020), in force from January 2022, are fully in line with this trend. Its objectives are to continue to reduce energy consumption, strengthen performance in summer comfort and continue to promote the production of decentralized renewable energy. For this reason, one of the most effective ways to reduce building energy consumption and emissions is to carry out energy performance monitoring and diagnostics for all existing buildings as well as the development of new buildings using low-emitting component materials. Another way to reduce energy consumption in buildings would be to develop biocomposite materials [3-5] to renew and improve indoor air quality, properly orient the building, use renewable energy and select suitable building materials. In this context, the energy recovery of waste and renewable resources plays an important role. Composites derived from agricultural by-products and bio-binders not only solve the problem of environmental pollution through the reuse of agricultural wastes but also contribute to protecting the environment by reducing CO_2 emissions during production and use as well as reducing the need for petroleum-based

composites. In particular, bamboo fibers are considered potential materials for making effective biocomposites because of their large availability, sustainability, durability, and hygrothermal properties [6, 7]. The biocomposites fabricated from bamboo fibers were reported as environmentally friendly materials [8-12]. Most of the studies evaluated the physicochemical properties, morphology, mechanical properties, and water absorption capacity of these materials [8, 11-16]. Some of them were considered insulation materials with a low thermal conductivity due to their low-density and highly porous structure. Although playing a fundamental role in thermal insulation performance, physicochemical, and hygrothermal properties, the evaluation of porosity and pore characteristics in bio-insulation materials has not received much attention. Yet, it is well-known that porosity and connectivity between pores have a direct effect on mass transfer properties [17]. In particular, the tridimensional observation and quantification of pores of these materials are still very limited, and most works focus on concrete-based materials. For example, the porosity could be obtained by identifying size parameters empirically from tomography images of concrete. The segmentation was performed by thresholding, and the porosity has been evaluated on a distinction between spherical and non-spherical pores [18]. Moreover, the porosity calculated from 2D and 3D images had no difference from experimental values obtained by Archimedes' principle-based method, performed by immersing the concrete in water [19]. These results evidence the validity of pore quantification by image processing techniques when the pore size distribution is consistent with the scans resolution. Besides, pore volumes have also been separated by pore throats. In this method, the shape of the pores was assigned to values

from 1 to 6, considering pore throats as ellipses. Hence, the major axis divided by the minor axis was calculated to express how close the pores are [20]. Moreover, the porosity has been determined by the average pores area of about 20 slices of 2D tomography images divided by the slice area, and no significant differences were found compared to the porosity from 3D images [20, 21].

To our knowledge, the pore characterization has not been extensively studied to provide an overview of biocomposites-based bamboo fibers. Therefore, in this work, we studied the porous properties of biocomposites from bamboo fibers and bamboo powders with PLA/PEG matrix using the X-ray tomography technique. The images obtained from this high-end device are processed to observe and quantify the 3D pores inside the materials. The distribution and orientation of bamboo fibers in the whole materials are also studied and reported.

2. Materials and methods

2.1. Materials

Poly(lactic) acid 4043D with 94% L-lactic acid content, a number-average molecular weight (M_n) of 67 kDa, the density of 1.24 g/cm^3, melt flow index of 0.6 g/min and the melting point of 145–160°C was purchased from NatureWorks LLC Co. Ltd (Minnesota, USA). Polyethylene glycol (PEG, M_w = 4000 g.mol^{-1}) was used as a plasticizer of pure PLA and purchased from Merck Co. (Germany). The bamboo fibers (*Bambusa stenostachya*) were collected at the Scientific Research Center for the Conservation of Natural Resources (PhuAn Bamboo Park, Vietnam). The bamboo fibers, from 1.0 to 2.0

cm in length and from 0.16 to 0.52 mm in diameter, were prepared by the mechanic method, as reported in a previous study [7]. The bamboo powders, about 0.1– 0.2 mm in diameter), were crushed from bamboo fibers as reported in the previous study [6].

2.2. Bamboo fibers treatment

To remove impurities, unexpected substances and improve the mechanical properties of biocomposites, bamboo fibers were pretreated with a NaOH solution. Firstly, the bamboo fibers were soaked in a 2% NaOH solution for 24 h at room temperature [22]. Then, they were taken out and washed thoroughly with distilled water until a neutral solution was obtained after washing (pH ≈ 7). Then, the fibers were dried at 60°C for 24 h before using for further experiments.

2.3. Fabrication of biocomposite materials

Biocomposites containing pure PLA, and bamboo fibers or bamboo powders were manufactured by the melting process method using a twin-screw Haake Polydrive device (Germany) with different components, as listed in Table 1. 10 wt.% PEG was used as the effective plasticizer for PLA as reported in the previous study [23]. Firstly, the components were preliminarily mixed and filled into a chamber mixer at a rotation speed of 60 rpm, at 170^{o}C for 10 min. Then, the mixture was shaped by an aluminum mold of 12×12×0.3 cm^3 using a hydraulic press at 185^{o}C, 50 kg/cm^2 for 15 min. The composite plates were then cooled to room temperature and kept in the mold for 24 h before removing them to avoid warping. Finally, the plates were then prepared for further characterizations.

Materials	PLA (wt.%)	bamboo fibers (wt.%)	bamboo powders (wt.%)
P100	100	0	0
PF30	70	30	0
PF40	60	40	0
PF50	50	50	0
PP40	60	0	40
PP50	50	0	50
PP60	40	0	60

Table 1: The compositions of biocomposites

2.4. Characterizations

2.4.1. Fourier transform infrared spectroscopy (FTIR)

The structure change of bamboo fibers after being treated with 2% NaOH solution was investigated by Fourier transform infrared (FT-IR) spectrometer Equinox 55 (Bruker Co., Germany) with an absorption mode at a resolution of 2 cm^{-1} in wavenumber ranges from

500 to 4000 cm^{-1}. The bamboo fibers were dried to remove the water vapor before being analysed.

2.4.2. Morphology assessment

The interfaces between matrix and bamboo fibers and the morphology of biocomposites were assessed using a scanning electron microscope (SEM, JSM 6600, JEOL Co., Japan). The cryo-fractured specimens were first coated with platinum and observed after freezing in liquid nitrogen.

2.4.3. 3D microstructure of biocomposites

The tridimensional microstructure of the composites was analyzed by combining X-ray tomography (EasyTom XL 150/160, RX-solutions, France) and image processing in the software Avizo 2019.1 (Thermo Fisher Scientific, USA). To obtain X-ray projections, samples were scanned using a micro-source, a CCD detector of 2004 ×1336 pixels and a voxel size of 5 μm. For these acquisition parameters, each scan lasted approximately 30 min and about 1100 projections were recorded. These images were processed in X-Act software 21.04.3 (RX-Solutions, France) and reconstructed to obtain image stacks, which were further analyzed in Avizo [24]. 3D volume visualization of the stacks was performed by applying the Volume Rendering tool (Colormap = “Grayscale”). Further, subvolumes (3 x 3 x 6 mm) were extracted from the original datasets and processed using a 3D Gaussian filter (Standard deviation = 1 px, kernel size = 2). After filtering, segmentation was performed in 3D using the Auto Thresholding tool (Auto Threshold Low, Mode = min-max, Criterion = Entropy) to identify sample pores. The obtained

binary images were analyzed using the Material Statistics function to calculate the pore volume fraction in the composites. In addition to that, the Labeling tool was applied to assign pores as individual particles, allowing the quantification of their volumes with the Label Analysis function. As fibers presented a similar intensity to the composite matrix, their segmentation could not be performed by automatic thresholding. Hence, in order to visualize their distribution in the composites, the Volume rendering tool was applied using a different colormap ("Physics") and a reduced opacity (0.02).

2.4.4. Thermal stability

The thermal stability of biocomposites was evaluated by Thermogravimetric analysis (TGA) using a TGA Q500 (TA Instruments, USA) under a nitrogen atmosphere. The heating rate was 10°C/min with a temperature range from 25 to 600°C.

2.4.5. Flexural properties

The flexural properties of biocomposites were characterized using a mechanical testing machine (Comtech, Taiwan). The specimen's dimension and testing protocol were prepared and performed according to ASTM D790. The obtained flexural results were the mean values of at least 5 measurements for each composite.

2.4.6. Water absorption

The water absorption of biocomposites was measured according to the ASTM D1348 standard. The specimens were immersed in water and mass change was monitored over time. Every 24h, the specimens were collected and their mass was weighed after the excess of water was wiped off from the surface. The measurement was stopped when the

specimen mass was constant (mass variation between two measurements less than 5%). The amount of water absorbed into specimens was an average value of at least 5 samples and calculated by the formula:

$$WA\ (\%) = 100 \times \frac{(m - m_0)}{m_0}$$

where WA (%) is water absorbed into specimen; m (g) is mass of specimen after immersing in water; and m_0 (g) is initial mass of specimen.

3. Results and discussions

3.1. Bamboo fibers treatment

FTIR technique is used to assess the chemical composition and structural changes in bamboo fibers before and after treatment with NaOH solution, as exhibited in Figure 1.

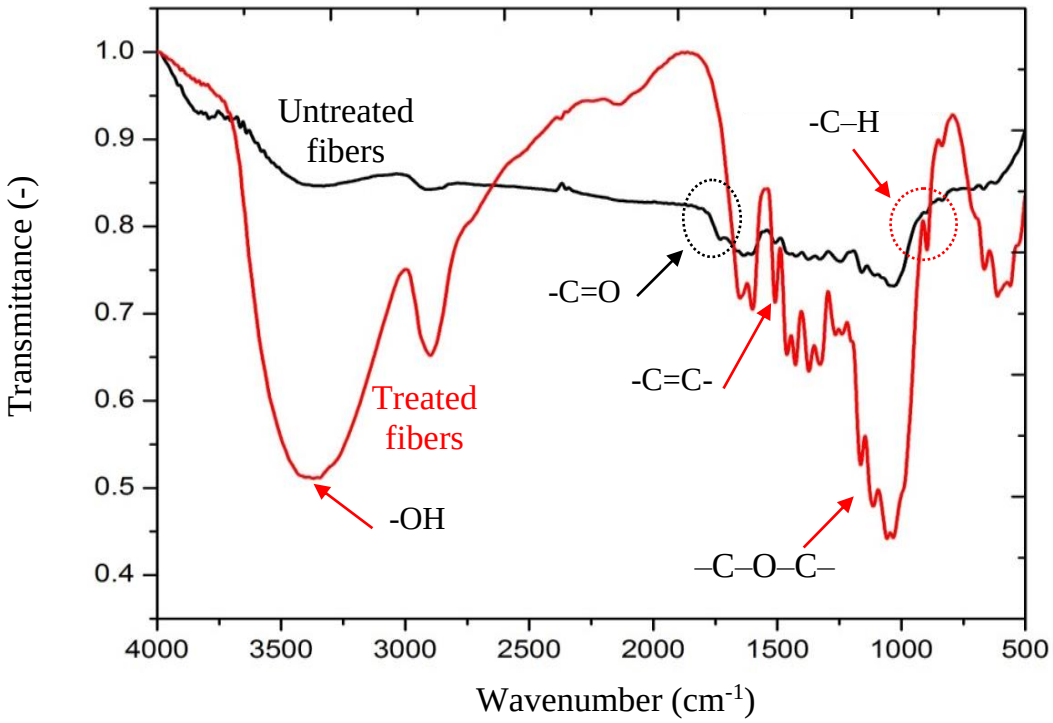

Figure 1. FTIR spectra of bamboo fibers before and after treating with NaOH solution

The FTIR spectrum of bamboo fibers before being treated with NaOH solution shows low-intensity overlapping peaks, which do not allow us to distinguish the typical vibrations of cellulose, hemicellulose, and lignin. However, the FTIR spectrum of the bamboo fibers treated with NaOH solution presents discrete peaks with high intensity, such as the band around 3000-3700 cm^{-1}, characteristic of the –OH groups present in the main constituents of bamboo fibers.

A low-intensity peak at 1732 cm^{-1} could not be observed in the FTIR spectrum of treated bamboo fibers. This peak could be associated with the oscillation of –C = O groups of acetyl and esters of hemicelluloses or with constituents from bamboo lignin, such as esters, ferulic and p-coumaric acids [25, 26]. A peak appears at a wavelength of 1508 cm^{-1}, representing the aromatic –C = C– stretching of the aromatic rings of lignin. The strong cellulose bands around 1113 cm^{-1} correspond to antisymmetric –C–O–C– bridge stretching. A change of a small peak is identified at 896 cm^{-1}, corresponding to –C–H deformation vibration in cellulose [26]. Thus, the FTIR spectrum of the bamboo fibers after treating with 2 wt.% NaOH solution shows that the impurities and a part of lignin and hemicelluloses were removed from bamboo fibers, which was intended to improve the bamboo fiber/matrix interface.

Furthermore, the FTIR spectra of biocomposites are exhibited in **Figure 2**. Accordingly, the oscillations observed from the FTIR spectra of biocomposites reinforced with treated bamboo fibers and powders do not differ because of the same interaction between bamboo and matrix PLA/PEG. This is also observed for the FTIR spectra of biocomposites with different bamboo fiber contents. However, the peak at 1735 cm^{-1}

representing carbonyl (C=O) stretching vibration peak does not appear in treated bamboo fibers but it is observed in all biocomposites. This result proves the creation of the chemical bonding between functional groups from PLA/PEG matrix and bamboo fibers. Furthermore, the intensity of this 1735 cm^{-1} peak does not change with bamboo fiber contents in biocomposites. It implies that the more addition of bamboo fibers does not change the chemical bonding of the PLA/PEG matrix and bamboo fibers during internal melt processing.

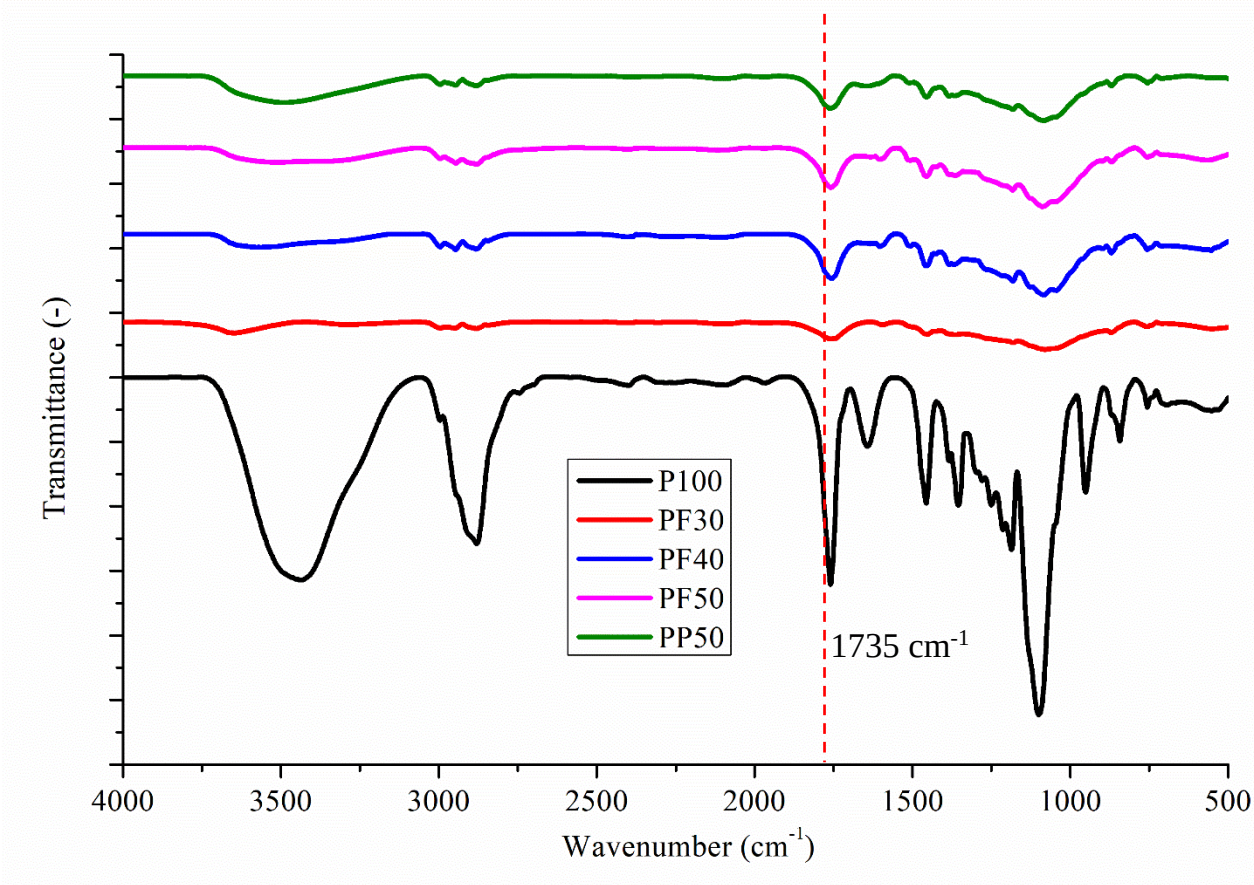

Figure 2. FTIR spectra of biocomposites

3.2. Flexural properties of biocomposites

The flexural properties of PLA-composites reinforced bamboo fibers and bamboo powders are presented in **Figure 3**. The PLA/PEG matrix has a flexural modulus and flexural strength of about 3273 MPa and 54.6 MPa, respectively. When the bamboo fibers are incorporated to the PLA/PEG matrix, the flexural modulus of these composites is significantly increased, while flexural strength is slightly improved. These values reach a peak at 40 wt.% of bamboo fibers in composite with approximately 5335 MPa for flexural modulus and 59.4 MPa for flexural strength, respectively. This result indicates that bamboo fibers presented a reinforcing role in the composites due to their higher flexural properties and stiffness than PLA/PEG matrix [16, 27]. However, when the bamboo fibers content is raised to 50 wt.%, the flexural modulus and flexural strength of the composite are reduced to about 3335 MPa and 52.4 MPa, respectively. It means that at 50 wt.% of bamboo fibers in the composite, the PLA/PEG matrix was not sufficient to wet all bamboo fibers to maintain a good adhesion at the interfaces between matrix and fibers [7, 16, 27].

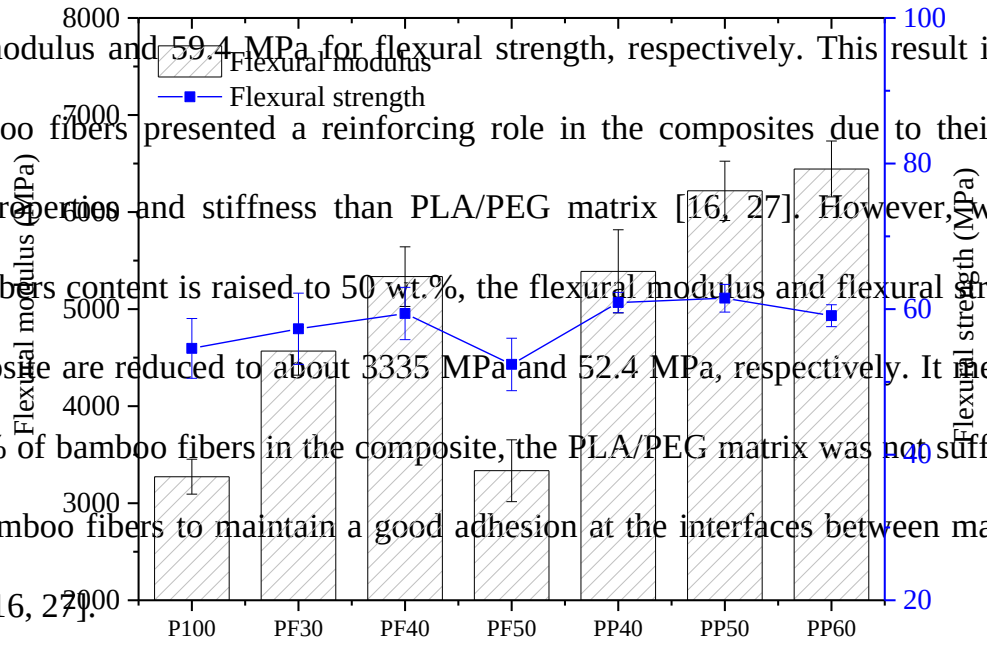

PF: PLA/PEG + treated bamboo fibers
PP: PLA/PEG + treated bamboo powders

Figure 3. Flexural properties of PLA-composites reinforced with bamboo fibers and bamboo powders at different contents.

On the other hand, the flexural properties of the PLA-composite reinforced with bamboo powders show a significant increase compared to with the reinforcement by bamboo fibers. This implies that bamboo powders exhibit a higher reinforcing role than bamboo fibers in PLA/PEG composite. Accordingly, the flexural modulus and flexural strength of PLA/PEG-composite reinforced of 50 wt.% bamboo powders are raised up 6219 MPa and 61.5 MPa, respectively, which are higher than that of PLA/PEG composite reinforced with bamboo fibers at 40 wt.%. This result may be surprising as the shape factor is important in composites, and we would expect the fiber composites to perform better than the powder composites. This observation is therefore probably explained by a better interface between matrix and particles in the case of powder: the smaller sizes of bamboo powders allow a more efficient mixing during the melting processing in the mixing chamber [6]. Moreover, with a smaller size than bamboo fibers, the bamboo powders are able to fill in the large voids in the composites, reducing the pore volume in the composite bulk and at interfaces between PLA/PEG matrix and bamboo powders. This result is consistent with the quantitative results of pore volume by tomography technique and image processing displayed in **Figure 6.**

However, when the bamboo powders content in composite increases to 60 wt.%, its flexural modulus still increases up to 6444 MPa. However, its flexural strength tends to

decrease to 59.1 MPa. This result shows a decrease in flexural strength when the reinforcement content in the composite is too high that the PLA/PEG matrix no longer exhibits as good adhesion as the composite with lower bamboo powder content (PP50). It means that the PLA/PEG matrix is not sufficient to wet all bamboo powders in this composite [7, 16, 27]. Therefore, in this study, the biocomposites reinforced with the high bamboo powders contents (> 50 wt.%) are not necessary and useful for further studies.

3.3. 3D visualization of bamboo fibers orientation in composites

3.3.1. 3D volume morphology

The 3D volume of the selected composites is reconstructed from a series of 2D images of each composite. The components of the composites including bamboo fibers, pores, and PLA/PEG matrix are distinguished by their density in the X-ray projections. **Figure 4** shows 3D volume reconstructions, corresponding to three PLA composites reinforced with bamboo fibers (PF30 and PF40) and bamboo powders (PP50).

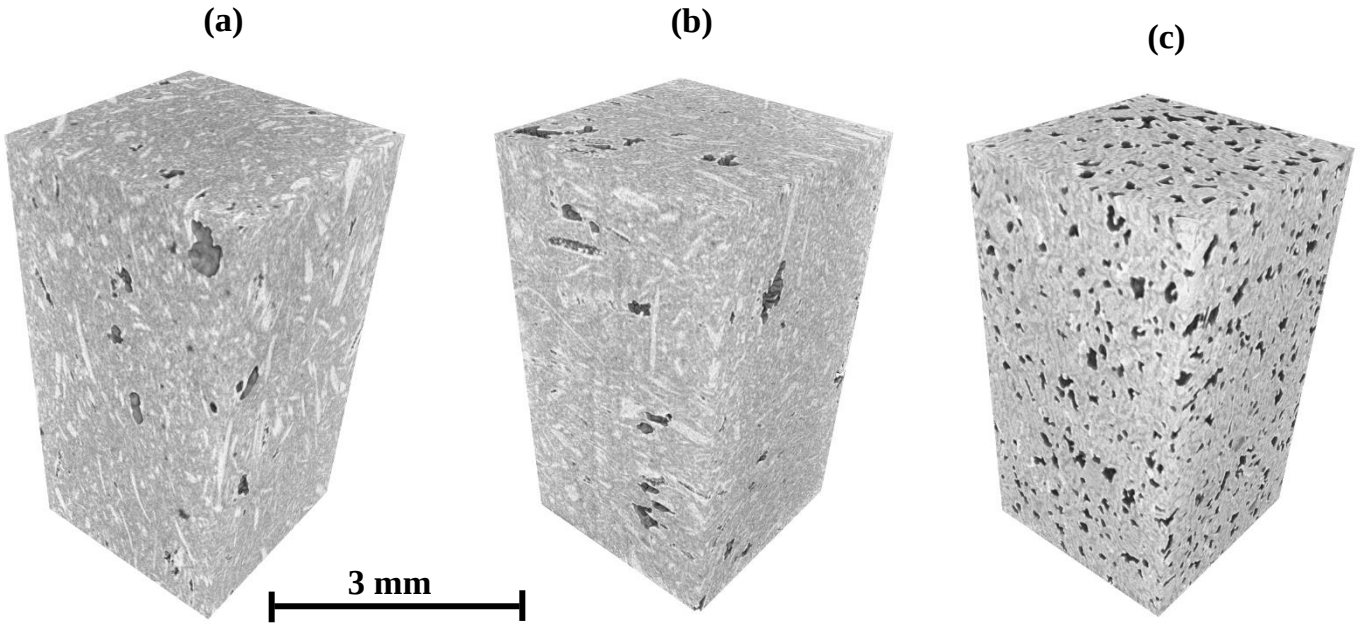

Figure 4: 3D volume reconstruction of PLA composites reinforced with: (a) 30 wt.% bamboo fibers, (b) 40 wt.% bamboo fibers and (c) 50 wt.% bamboo powders.

These 3D volumes represent the bamboo fibers, pores, and the PLA/PEG matrix, which are distinguished by their different intensities in the grayscale colormap. Accordingly, **Figures 4a and 4b** allow the components inside the composites to be observed, whereby the gray represents PLA/PEG matrix; white lines with different sizes represent bamboo fibers, and pores with different sizes and shapes are represented by the color black. Furthermore, **Figure 4c** also allows to observe the shape and distribution of the pores in composites (PP50).

The 3D volume morphology of the composite containing 30 wt.% (PF30) bamboo fibers exhibits very few pores, which are scattered throughout the sample. This is due to the low content of bamboo fibers, so the matrix has completely covered the whole fibers and filled the gaps inside this composite. When the fiber content is increased to 40 wt.% (PF40), the pores appear in larger size due to the rigidity of bamboo fibers. For the composite containing 50 wt.% bamboo powders (PP50), the pores are more abundant but evenly distributed throughout the sample. However, the pores seemed to be smaller in size compared to composites containing 40 wt.% bamboo fibers. This is explained by the small size of bamboo powders allowing the matrix to better penetrate during fabrication.

3.3.2. 3D fibers orientation

X-ray tomography and image processing techniques also allow us to visualize the distribution and orientation of bamboo fibers within the composites, as presented in **Figure 5**. Accordingly, the images of the PLA/PEG composite containing 30 wt.%

bamboo fibers (PF30) show that the bamboo fibers are randomly distributed and display multiple orientations. They are not arranged in an orderly manner inside this composite. The bamboo fibers are observed with different sizes in the form of bundles of interwoven or stacked fibers. Besides, spaces between the adjacent fibers could also be observed.

When the bamboo fibers content was increased to 40 wt.% (Figure 5b), the fibers remained randomly dispersed and more fiber agglomeration could be observed due to an increase in the number of fibers in this composite. The fibers sizes could still be visualized, however, compared to the PF30, the spaces between the fibers could not be identified. Indeed, the bamboo fibers are mainly presented as folded lines and curves in the composite. Bamboo fibers distribution could be affected by mixing time and fiber

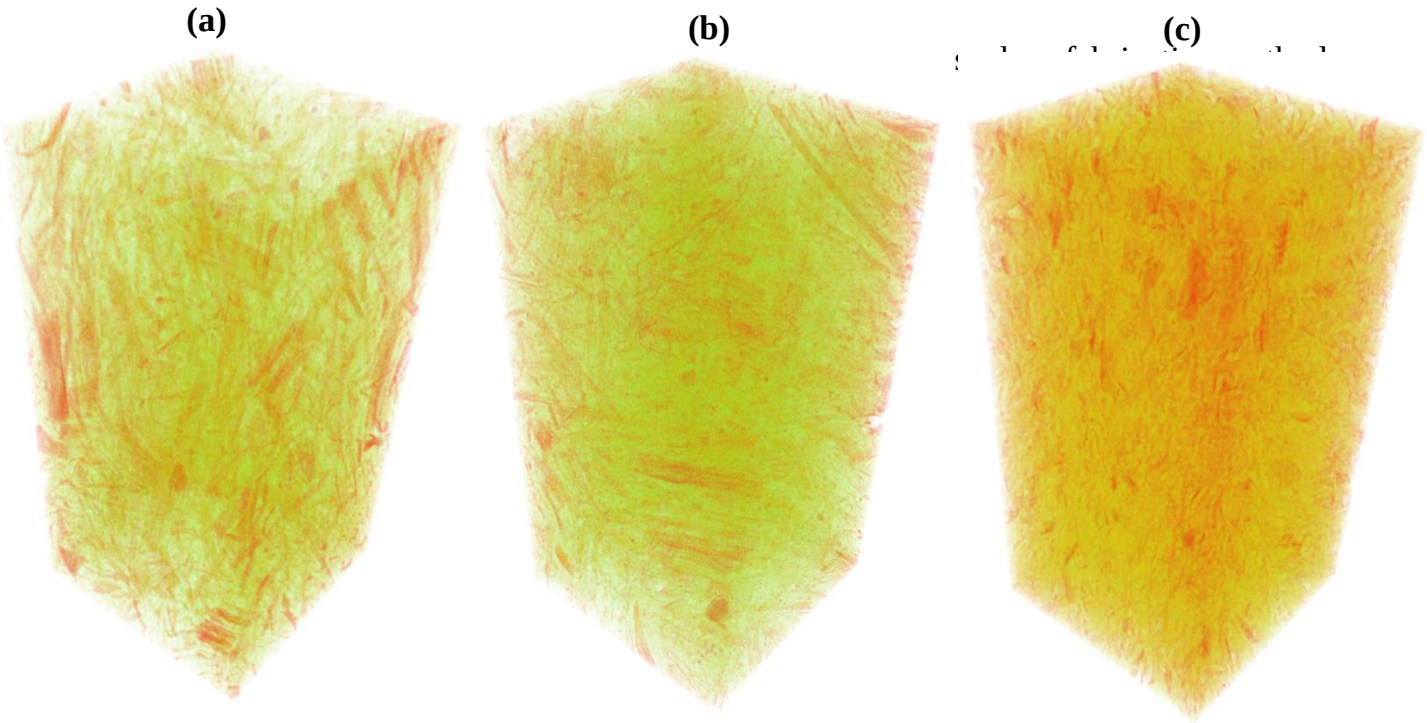

Figure 5: 3D bamboo fibers orientation in composites: (a) PF30, (b) PF40, and (c) PP50

In the composite containing 50 wt.% bamboo powders (**Figure 5c**), the bamboo powders density is high. Particles tend to agglomerate and the distance between the grain boundaries is not observed. Moreover, the particles size is also indistinguishable. This is due to the excessive bamboo powders loading and the applied tomography resolution, which does not allow the observation of bamboo powder size.

3.3.3. 3D visualization of pore distribution

The pore size distribution and pore volume fraction are two fundamental parameters to express the pore characteristics. The pore size distribution has been studied in 3D and the pixel (or voxel) number count is the most convenient size measurement method. The 3D visualization of segmented pores in the composites is presented in **Figure 6**. In these images individual pores are represented with different colors.

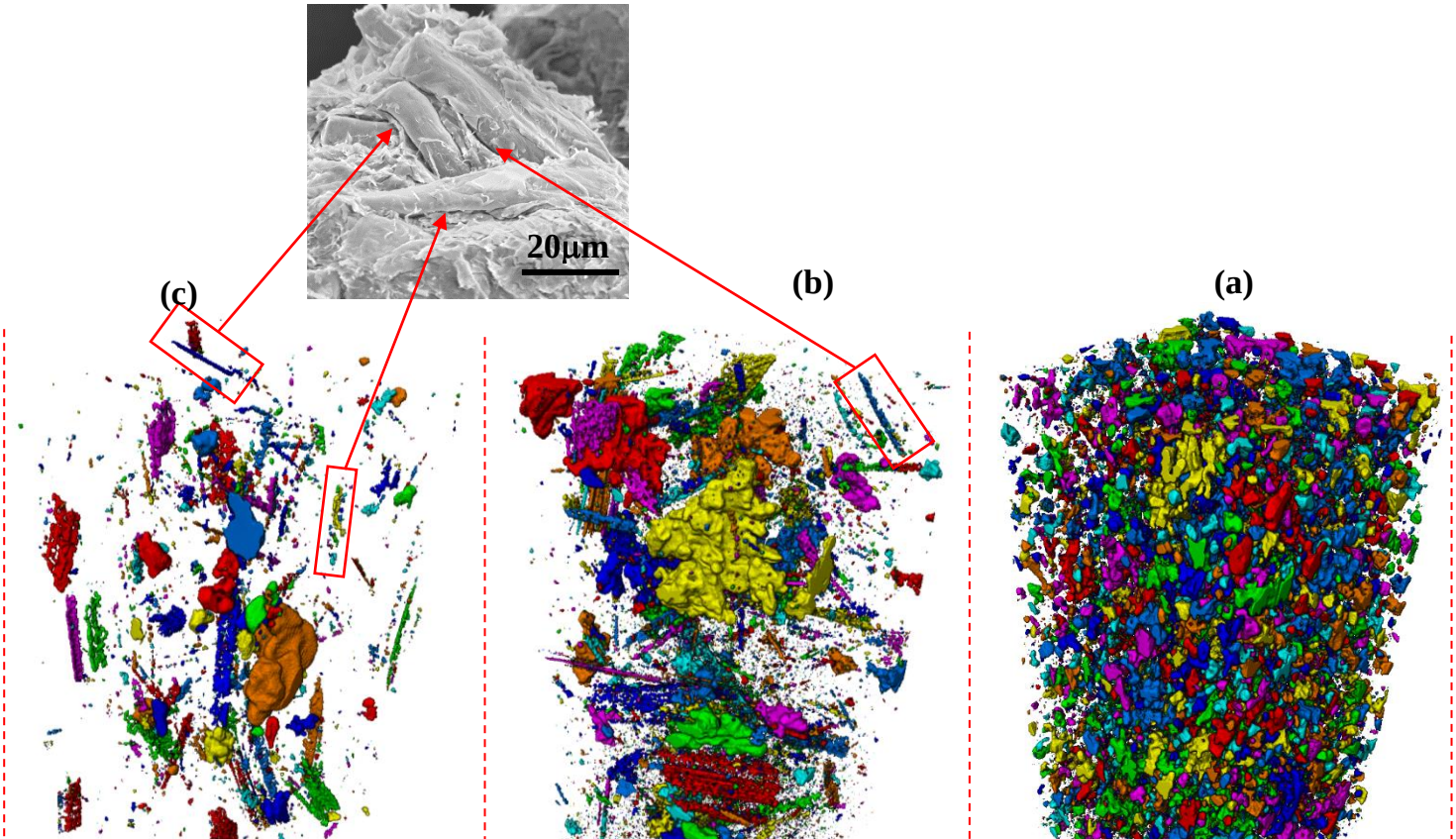

Figure 6: 3D visualization of pore in the composites: (a) PF30, (b) PF40, and (c) PP50

For the PF30 sample, the pore quantity is low, the pores are unevenly distributed inside the composites, and small pores are clustered together in longitudinal arrays. This is explained by the porosity formed at the interface between the bamboo fibers and the matrix. This result is confirmed through the inserted 2D SEM image and depicted through the red arrows in **Figure 6**. The pore distribution in three composites are also investigated as reported in **Figure 7**.

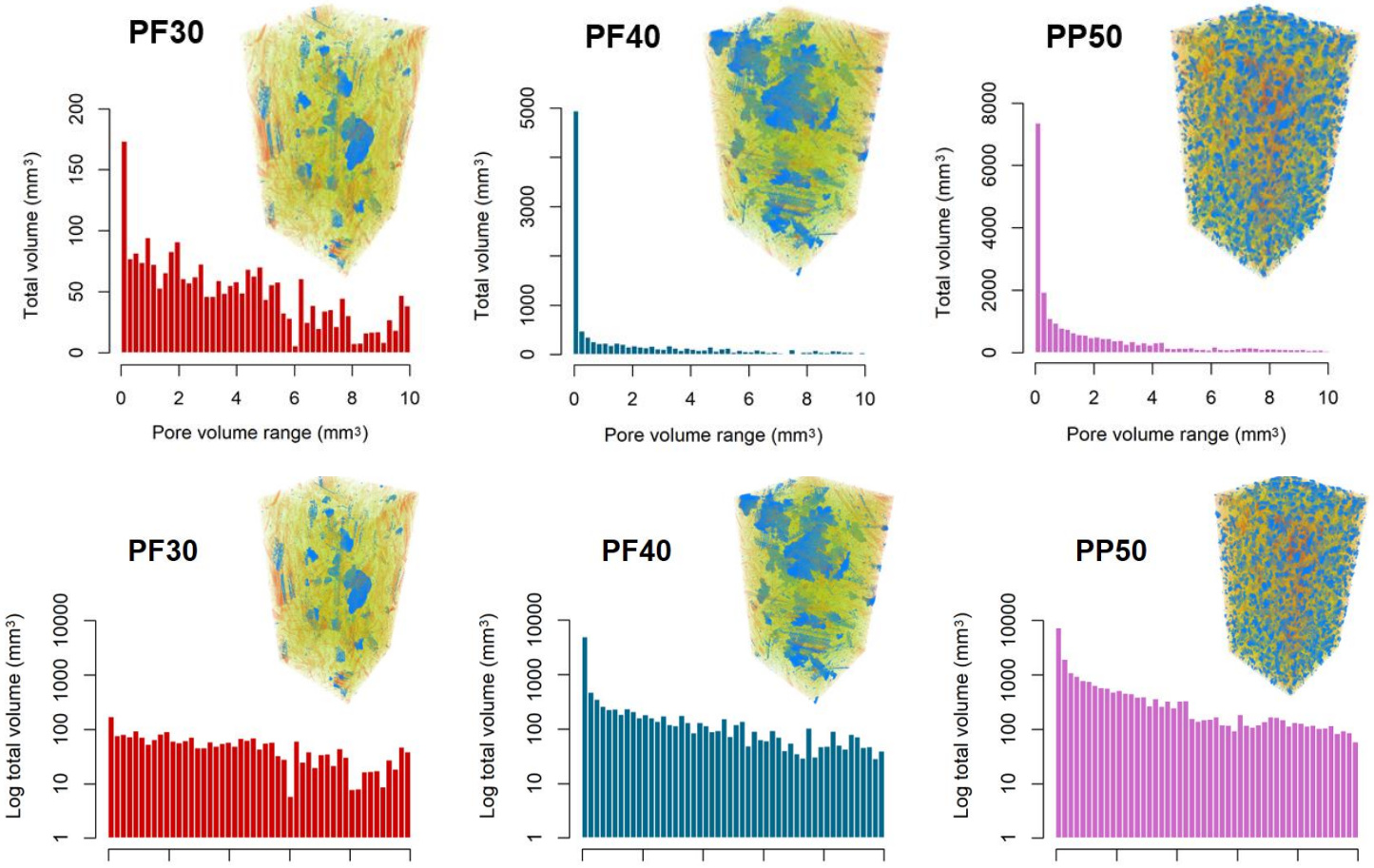

Figure 7: Pore distribution and total volume pore per category in the composites with linear and log scales

In order to avoid the huge number of small pores, the categories were quantified by their cumulated volumes. For a better appreciation of these distributions, we proposed both a linear and log scales. This figure confirms that the total porosity is very small for sample PF30, with a slightly decreasing distribution of volume per category over the total range, 0 to 10 mm^3. Sample PF40, depicts a huge increase of small pores (5000 mm^3 instead of 170 mm^3 for the first category: 0-0.2 mm^3), but also large volumes of medium-size pores and a significant presence of large pores, as can be seen on the images. At this level of solid fraction, this is explained by the rigidity of fibers that might preserve cavities, either during forming in the internal mixer or by subsequent relaxation. In addition, the pore features could also be affected by the characteristics of fibers. For instance, the shape of pores showed a tendency from spherical to oval with fibers due to the distortion of the matrix [29]. The bar graph of PP50 composite confirms the large porosity, but with regular spatial distribution of pore size. Compared to the previous distributions, the huge increase of small- and medium-size pores (up to 4 mm^3) is obvious. Above this value, contrary to the previous samples, a rapid drop in category volumes is observed for large pores, especially visible on the linear scale.

This partition and amount or porosity points out the role of the particle size: large and long particles are likely to produce a small number of large pores due to the stiffness of biomass. They build up weakness points at high mass fractions and explain the poor mechanical behavior, which seems contradictory with the positive effect of the shape ratio of particles. On the contrary, with powder, the porosity might be large, again as a function of mass fraction, but the pores remain of average size and remain evenly distributed in space. In conclusion, the particle size matters more than the shape ratio for high particle/PLA ratios. This explains the apparently paradoxical behavior of the mechanical properties.

The total volume pore per category of three samples was also plotted in **Figure 7** to correct the bias in number of pores, generally much larger for small pores. The partition of volume per category confirms a small porosity for PF30, which is consistent with total value reported in Table 2. PF40 has an increased porosity but keeps a similar balance between small and large pores. The bamboo powders composite, PP50, presents the largest total porosity, but, contrary to the fiber sample, the proportion of small pores is larger, even when quantified in terms of volume rather than number. This depicts a much regular pore distribution, likely to explain the best mechanical performances. This is even more meaningful if, in addition to this observation, we keep in mind that the larger the pore volume, the higher the presence of interconnected pores, which are counted as one large pore by the software. This is also confirmed by the increased kinetic in water uptake result.

The pore volume fraction of the 3 biocomposites is also calculated based on the cumulated pore volume from the composites and presented in Table 2. The PF30 sample has a very low porosity, about 0.87%, the PF40 sample has a porosity of about 2.73% and the PP50 sample has a porosity of about 12.12%. When the bamboo fibers content in composites is increased, the porosity increases because of increasing in the rigidity of fibers. This result is also consistent with the concrete materials in the literature, indeed, the porosity of the concrete containing polypropylene fibers increased alongside fiber's content [30]. Furthermore, these values are consistent with the number and volume of pore observed in **Figure 7**. It could be observed that the porosity of biocomposites is increased with biomass content, whatever it is fiber or powder. However, the smaller pore size and better distribution obtained with powder composite is likely to explain the best mechanical performances.

Table 2: The pore volume fraction of composites

Material	Porosity (%)
PF30	0.87
PF40	2.73
PP50	12.12

4. Thermal stability of biocomposites

The thermal stability of the PLA/PEG matrix and its composites is shown through the TGA curves, as illustrated in **Figure 8**. Firstly, the thermal decomposition curve of the PLA/PEG matrix shows a single step with an initiation temperature at about 311^{o}C and

complete temperature at about 490°C with a residue nearly zero. The thermal decomposition of composite reinforced with 40 wt.% bamboo fibers (PF40) has two distinct thermal decomposition steps. The first step with starting and ending decomposition temperatures seems to coincide with the thermal decomposition step of the PLA/PEG matrix. This is thought to be the thermal decomposition of the PLA/PEG matrix in the composite. The second thermal decomposition step starts at about 390°C and ends at about 500°C, which is the decomposition temperature of the reinforced bamboo fibers component in this sample. The residue after thermal decomposition remains about 10%. Thus, reinforcing bamboo fibers into PLA/PEG matrix tends to increase the thermal stability of this composite due to the higher thermal decomposition of bamboo fibers compared to PLA/PEG matrix.

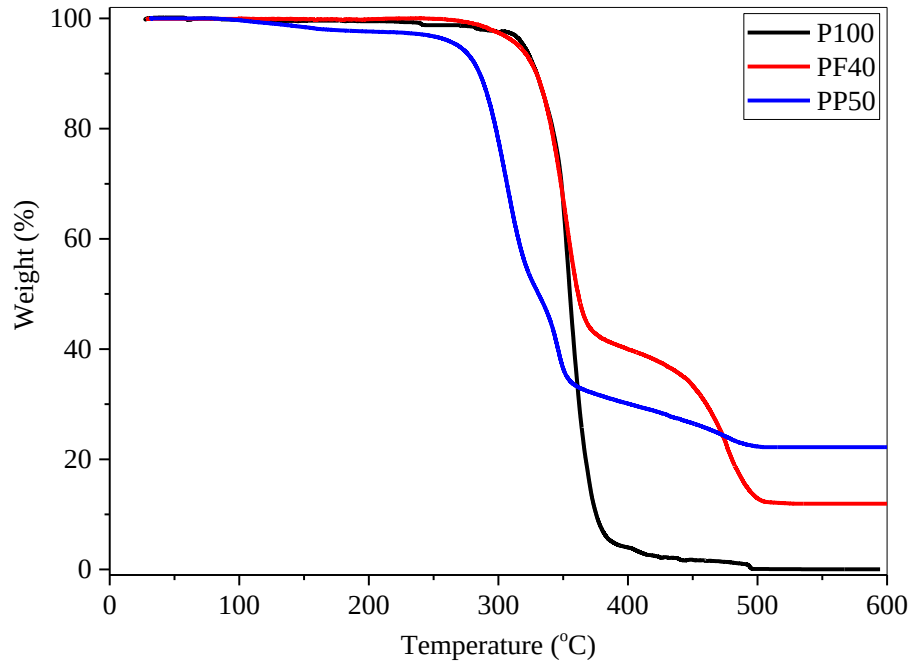

Figure 8: Thermal decomposition curves of biocomposites

The thermal stability of PLA/PEG reinforced with 50 wt.% bamboo powders (PP50) is reduced compared to the PLA/PEG matrix. Accordingly, the first decomposition is observed before 150^{o}C, which is the decomposition of low molecular weight and volatile substances. In fact, the bamboo exists in powders form with small sizes (< 20 micrometers), containing compounds which are easily decomposed by heat. Therefore, the decomposition weight of this step is about 5%. The thermal decomposition starts at about 260^{o}C and ends at 350^{o}C, this is thought to be the thermal decomposition of PLA/PEG mixed with bamboo powders with a lower temperature than PLA/PEG only. This result is due to the lower thermal stability of bamboo powders compared to PLA/PEG matrix. Moreover, the first parts of the curves are completely similar for net PLA/PEG and PF40, as if PLA is likely to protect fibers. The large porosity of PP50 could explain that this protective effect doesn't exist for powder. The second decomposition step starts at about 350^{o}C and ended at 500^{o}C, corresponding to the thermal decomposition of the heat-stable components in bamboo powders. The residual of this sample after thermal decomposition is about 20%.

The powders appear to be agglomerated in the tomography images. Maybe the small pores in the image could be caused by the emission of volatile compounds during the composite fabrication, generating bubbles in the matrix that are trapped after cooling and solidification of the polymer. It could be explained due to mechanical relaxation, indeed, when the level of fiber increases and pore formation occurs due to the relaxation of bend fiber, that leads to large pore because bending deformation is large. However, in the PP50

sample, the relaxation occurs more to release cell compression, which generates smaller-distributed pores of similar volume.

Moreover, maybe the NaOH treatment only modifies fibers on the surface. The interior, which is revealed after the powders are crushed, may still present volatile substances, which we see in the TGA and can be emitted during extrusion, generating bubbles that could result in the porous structure observed by tomography.

5. Water absorption

The water absorption capacity of the biocomposites is shown in **Figure 9**. The PLA/PEG matrix exhibits a good water resistance, corresponding to the lowest and seemingly negligible water absorption, less than 0.6% for 11 days. The water absorption capacity of biocomposites increases with the increasing loading contents and experimental time. Indeed, the composite containing 30 wt.% bamboo fibers absorbs about 9% and reaches the water saturation after 9 days of test. The same water saturation period for the sample which contains 40 wt.% bamboo fibers with the water absorption maximum of about 11%. The composite containing 50 wt.% bamboo powders (PP50) has the highest hygroscopicity with a water absorption amount of about 13% and reached water saturation after 5 days. These results imply that bamboo fibers and bamboo powders have increased the hygroscopicity of the biocomposites. Interestingly, the quantity of absorbed water directly depends, with values of 30%, 27.5% and 26% respectively for PF30, PF40 and PP50.

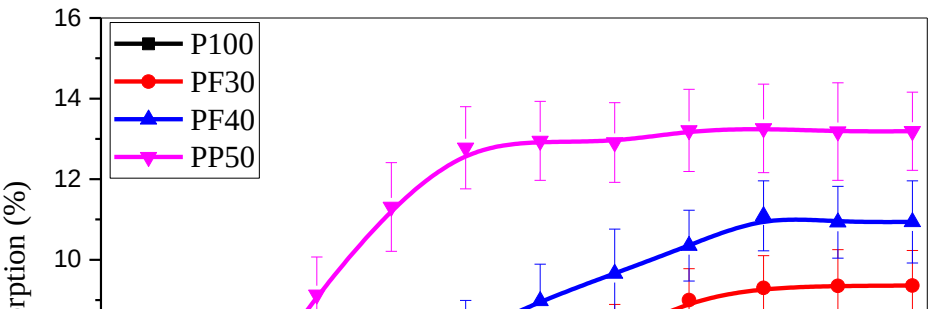

Figure 9: Water absorption ability of biocomposites

Regarding the imbibition dynamic, the two fiber composites depict the same trend, which indicates that the few large pores of PF40 are not connected. On the contrary, the faster dynamic of the bamboo powders composite indicates the numerous average-size pore are connected and allow water to percolate in this pore network.

Conclusion

Biocomposites from bamboo fibers, bamboo powders and PLA/PEG matrix have been fabricated by melting method. The flexural properties of the materials are optimal at 40 wt.% bamboo fibers, but is higher, 50 wt.%, for bamboo powders. This result was explained by 3D observations, using an x-ray tomography. 3D volume reconstruction, fiber orientation and pore characteristics of composite materials such as volume fraction and size distribution have been determined by image processing using the Avizo software. Accordingly, the porosity of the materials increases with the content of the bamboo reinforcement phase. More specifically, the composite material containing 50

wt.% bamboo powders has numerous pores of average size, well distributed spatially, while that of bamboo fibers have a few numbers of large pores, likely to explain the difference of mechanical behavior. Consistently with the water-uptake capacity of bamboo, the water absorption of the composite material increases linearly with the content of the bamboo reinforcement phase. In addition, the average-size pores in the powder composite are sufficiently numerous to percolate and significantly accelerate the dynamic of water uptake.

Acknowledgments

This research is funded by Vietnam National University HoChiMinh City (VNU-HCM) under grant number QGB11.ĐA 01.

Conflicts of Interest: The authors declare no conflict of interest.

References

[1] M. Jang, T. Hong, C. Ji, Hybrid LCA model for assessing the embodied environmental impacts of buildings in South Korea, Environmental Impact Assessment Review 50 (2015) 143-155.
[2] T. Hong, D. Kim, C. Koo, J. Kim, Framework for establishing the optimal implementation strategy of a fuel-cell-based combined heat and power system: Focused on multi-family housing complex, Applied Energy 127 (2014) 11-24.
[3] L. Liu, H. Li, A. Lazzaretto, G. Manente, C. Tong, Q. Liu, N. Li, The development history and prospects of biomass-based insulation materials for buildings. , Renewable and Sustainable Energy Reviews 69 (2017) 912-932.
[4] M. Palumbo, A.M. Lacasta, M.P. Giraldo, L. Haurie, E. Correal, Bio-based insulation materials and their hygrothermal performance in a building envelope system (ETICS), Energy and Buildings 174 (2018) 147-155.
[5] D. Maskell, C.F. da Silva, K. Mower, C. Rana, A. Dengel, R.J. Ball, A. Shea, Properties of bio-based insulation materials and their potential impact on indoor air quality, Academic Journal of Civil Engineering, 33(2) (2015) 156-163.
[6] D.M. Nguyen, A.-C. Grillet, Q.-B. Bui, T.M.H. Diep, M. Woloszyn, Building bio-insulation materials based on bamboo powder and bio-binders, Construction and Building Materials 186 (2018) 686-698.

[7] D.M. Nguyen, A.-C. Grillet, T.M.H. Diep, C.N. Ha Thuc, M. Woloszyn, Hygrothermal properties of bio-insulation building materials based on bamboo fibers and bio-glues, Construction and Building Materials 155 (2017) 852-866.
[8] F. Rao, Y. Ji, N. Li, Y. Zhang, Y. Chen, W. Yu, Outdoor bamboo-fiber-reinforced composite: Influence of resin content on water resistance and mechanical properties, Construction and Building Materials 261 (2020) 120022.
[9] M. Jawaid, S. Awad, H. Fouad, M. Asim, N. Saba, H.N. Dhakal, Improvements in the thermal behaviour of date palm/bamboo fibres reinforced epoxy hybrid composites, Composite Structures 277 (2021) 114644.
[10] Y. Hu, F. Hu, M. Gan, Y. Xie, Q. Feng, Facile one-step fabrication of all cellulose composites with unique optical performance from wood and bamboo pulp, Carbohydrate Polymers 274 (2021) 118630.
[11] M.L. Sánchez, W. Patiño, J. Cárdenas, Physical-mechanical properties of bamboo fibers-reinforced biocomposites: Influence of surface treatment of fibers, Journal of Building Engineering 28 (2020) 101058.
[12] T. Bai, D. Wang, J. Yan, W. Cheng, H. Cheng, S.Q. Shi, G. Wang, G. Han, Wetting mechanism and interfacial bonding performance of bamboo fiber reinforced epoxy resin composites, Composites Science and Technology 213 (2021) 108951.
[13] Y. Hu, F. Hu, M. Gan, Y. Xie, Q. Feng, A rapid, green method for the preparation of cellulosic self-reinforcing composites from wood and bamboo pulp, Industrial Crops and Products 169 (2021) 113658.
[14] Z. Qiu, J. Wang, H. Fan, Low velocity flexural impact behaviors of bamboo fiber reinforced composite beams, Polymer Testing 94 (2021) 107047.
[15] A.B.M. Supian, M. Jawaid, B. Rashid, H. Fouad, N. Saba, H.N. Dhakal, R. Khiari, Mechanical and physical performance of date palm/bamboo fibre reinforced epoxy hybrid composites, Journal of Materials Research and Technology 15 (2021) 1330-1341.
[16] R.B. Yusoff, H. Takagi, A.N. Nakagaito, Tensile and flexural properties of polylactic acid-based hybrid green composites reinforced by kenaf, bamboo and coir fibers, Industrial Crops and Products 94 (2016) 562-573.
[17] Louërat M., Ayouz M., Perré P., Heat and moisture diffusion in spruce and wood panels computed from 3-D morphologies using the Lattice Boltzmann method, Journal of Thermal Science 130 (2018) 471-483.
[18] A. du Plessis, W.P. Boshoff, A review of X-ray computed tomography of concrete and asphalt construction materials, Construction and Building Materials 199 (2019) 637-651.
[19] F. Wen, H. Fan, S. Zhai, K. Zhang, F. Liu, Pore characteristics analysis and numerical seepage simulation of antifreeze permeable concrete, Construction and Building Materials 255 (2020) 119310.
[20] F. Yu, D. Sun, M. Hu, J. Wang, Study on the pores characteristics and permeability simulation of pervious concrete based on 2D/3D CT images, Construction and Building Materials 200 (2019) 687-702.

[21] J. Zhang, G. Ma, R. Ming, X. Cui, L. Li, H. Xu, Numerical study on seepage flow in pervious concrete based on 3D CT imaging, Construction and Building Materials 161 (2018) 468-478.
[22] Q.B. Bui, J. Colin, T.D. Nguyen, N.D. Mao, T.M.L. Nguyen, P. Perré, Mechanical and thermal properties of a biocomposite based on polyvinylchloride/epoxidized natural rubber blend reinforced with rice husk microfiller, Journal of Thermoplastic Composite Materials 34(9) (2019) 1180-1192.
[23] T.P.T. Nguyen, D.V. Nguyen, C.N.H. Thuc, Q.B. Bui, P. Perré, D.M. Nguyen, Valorization of starch nanoparticles on microstructural and physical properties of PLA-starch nanocomposites, Journal of Applied Polymer Science 139(10) (2022) 51757.
[24] P. Perré, D.M. Nguyen, G. Almeida, A macroscopic Washburn approach of liquid imbibition in wood derived from X-ray tomography observations, Scientific Reports 12(1) (2022) 1750.
[25] R. Li, J. Fei, Y. Cai, Y. Li, J. Feng, J. Yao, Cellulose whiskers extracted from mulberry: A novel biomass production, Carbohydrate Polymers 76(1) (2009) 94-99.
[26] S. Elanthikkal, U. Gopalakrishnapanicker, S. Varghese, J.T. Guthrie, Cellulose microfibres produced from banana plant wastes: Isolation and characterization, Carbohydrate Polymers 80(3) (2010) 852-859.
[27] S.C. Chin, K.F. Tee, F.S. Tong, H.R. Ong, J. Gimbun, Thermal and mechanical properties of bamboo fiber reinforced composites, Materials Today Communications 23 (2020) 100876.
[28] Y. Qin, H. Wu, Y. Zheng, W. Wang, Z. Yi, Microscopic Texture of Polypropylene Fiber-Reinforced Concrete with X-Ray Computed Tomography, Advances in Civil Engineering 2019 (2019) 2386590.
[29] J.D. Ríos, C. Leiva, M.P. Ariza, S. Seitl, H. Cifuentes, Analysis of the tensile fracture properties of ultra-high-strength fiber-reinforced concrete with different types of steel fibers by X-ray tomography, Materials & Design 165 (2019) 107582.
[30] T. Simões, H. Costa, D. Dias-da-Costa, E. Júlio, Influence of fibres on the mechanical behaviour of fibre reinforced concrete matrixes, Construction and Building Materials 137 (2017) 548-556.